Proceedings of the 2003 IEEE/RSJ
Intl. Conference on Intelligent Robots and Systems
Las Vegas, Nevada · October 2003

Biomimetic Propulsion for a Swimming Surgical Micro-Robot

Jon Edd[1†], Sébastien Payen[1†], Boris Rubinsky[1], Marshall L. Stoller[2], and Metin Sitti[3]

[1]Department of Mechanical Engineering, University of California, Berkeley, CA 94720
[2]Department of Urology, University of California, San Francisco, CA 94143
[3]Dept. of Mechanical Eng. and Robotics Institute, Carnegie Mellon University, PA 15213
{jonedd, spayen, rubinsky}@me.berkeley.edu, mstoller@urol.ucsf.edu, sitti@cmu.edu

Abstract-- A surgical micro-robot that swims inside the human ureter is proposed to provide a novel and minimally invasive method of kidney stone destruction. Inspired by the swimming mechanisms of bacteria such as E. coli, the robot utilizes biomimetic synthetic flagella composed of multiwalled carbon nanotubes that are driven into a rotating helical shape by a micro motor. Design aspects are discussed with the focus on locomotion. The performance of the propulsion mechanism is determined through simultaneous modeling of the viscous drag on the filaments and the stress strain behavior of the nanotubes. The effects of the synthetic flagellum geometry and frequency of rotation on efficiency and swimming speed are explored. With 1nW of power, utilizing 100μm-long filaments, swimming speeds approaching 1 mm/s are shown to be possible for a realistic design. The proposed new robot would revolutionize kidney stone destruction if implemented, yet the design of the robot and the propulsion analysis are applicable to many other possible surgical procedures.

I. INTRODUCTION

This paper presents the design of a robot that swims inside the human ureter to destroy kidney stones non-invasively. In order to accomplish this, the robot has to maneuver through the urethra and into the bladder, then enter the correct ureter and find the kidney stones. Once it has found them, it needs to be capable of destroying the stones without adverse effects to the surrounding tissue. Upon completion of its task, it must exit the body safely. The duration of the procedure should be similar to that of other stone removal techniques. The design of the robot is presented as a total system. Major functions include sensors, a power source, means of communication, control, packaging, stone destruction and propulsion. This paper primarily focuses on the design of the propulsion mechanism.

Research into swimming micro-robots for *in vivo* applications faces many challenges, of which a means of propulsion and a power source are two primary concerns. In order to design propulsion systems that work at the micro scale, it is instructive to look at how nature has accomplished this. In the Stokes flow regime present in microscopic viscous media, bacteria and spermatozoa use flagella and cilia to swim. Flagella and cilia range from 18nm to half a micron in diameter and from a few hundred nanometers in length for cilia to 200μm for flagella. For these systems, propulsion is achieved through effective use of the viscous drag produced from the spinning tail. Due to the extremely small Reynolds number in this flow regime, inertial terms are negligible. Whereas typical motors exhibit undesirable effects due to the increased influence of viscosity, flagella and cilia depend completely on this to function.

A micro-robot swimming inside the body to destroy kidney stones is proposed in this paper for the first time. Guo et al. [1, 2] developed a swimming robot a few centimeters long that uses polymer actuators [3], sensors and a power source. The idea to destroy kidney stones with a micro-robot contains several advantages as compared with traditional methods such as lithotripsy or surgery [4]. Destruction of the stone would be possible with more selectivity and less overall damage to the kidney. It would also provide more flexibility in choosing the optimum mechanism of stone destruction. Importantly, the potential applications of the proposed micro-robotic system are not limited to the treatment of kidney stones: the insights gained for propulsion in particular could be employed in drug delivery to specific organs.

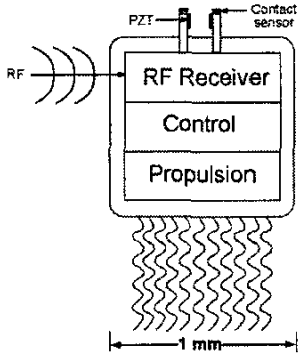

Figure 1: Overall design of swimming micro-robot.

II. DESIGN

In order to understand the interaction between each system inside the micro-robot and also between the micro-robot and the surrounding medium, it is simplest to represent the system in a functional structure as shown in Figure 2. This graph identifies all the sources of energy, materials and signals that will enter and leave the system.

† The first two authors contributed equally.

0-7803-7860-1/03/$17.00 © 2003 IEEE

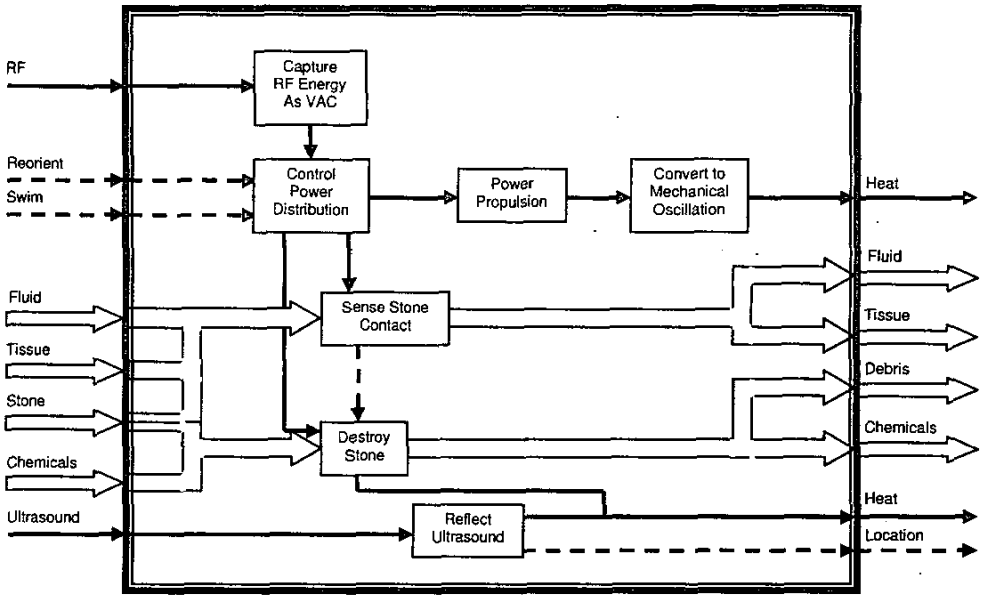

Figure 2: Function structure of the swimming micro-robot system. Solid lines represent flow of energy, dashed lines and block arrows represent signals and materials respectively

The robot is composed of five parts as shown in Figure 1. Three components will interact with the surrounding fluid: the packaging, the synthetic flagella that propel the robot, and the destruction mechanism (chemically active needles or an ultrasound system). Conversion of electric potential into mechanical work via two orthogonal comb drives per motor will drive the circular translation of the CNTs, and the control system will distribute the energy in order to provide maneuverability. Finally, a radio frequency receiver [5] or a thin wire will allow communication with the outside and provide power for the destruction mechanism.

The robot body should have a cylindrical shape roughly 1mm in diameter and be as smooth as possible to allow painless entry into the different vessels of the renal system (urethra and ureter). As this robot will function inside the human body, it is important that its whole structure be biocompatible. The time of operation should not be too much longer than five hours, which is similar to the duration of other methods to destroy kidney stones. Finally, the destruction mechanism should not be dangerous for the organism and should be sufficiently powerful to destroy kidney stones or at least fragment them into small debris.

III. Nomenclature

To simplify the understanding of the equations and formulations presented, a list of variables is presented here in order of occurrence.

Re	Reynolds number
ρ	density
μ	viscosity
U	speed of the robot
R	effective radius of the robot
p	pressure
$\mathbf{u}$	filament velocity vector
ΔT	period of filament motion
L	length of filament
$\mathbf{f}(f_x, f_y, f_z)$	force per unit length acting on filament
l	arc length along filament
t	time
$\mathbf{e}_x, \mathbf{e}_y, \mathbf{e}_l, \mathbf{e}_n$	unit vectors in the coordinate directions
$\mathbf{r}$	radius vector from x axis to filament
C_D	coefficient of drag in x direction
$C_{D\Omega}$	coefficient of drag for rotation of robot
Ω	angular rotation rate of robot
ω	angular rotation rate of filament
θ	helix angle
f_l, f_n	force per unit length tangent and normal to filament
N	number of filaments
λ	helical wavelength of filament
A	helical amplitude of filament
C_l, C_n	RFT coefficients
b	radius of filament
F	thrust force produced from filaments
T	torque generated by robot
η	efficiency of propulsion
τ, κ	Frenet torsion and curvature

IV. FLUID MECHANICS MODELING

A. The Micro-Fluidics

In order to treat the fluid modeling as Stokes flow, it must be shown that the Reynolds number is small. The robot will be in contact with the fluid inside the renal system during the whole operation, and the viscosity and density of urine are similar to that of water at body temperature. Given the millimeter-scale of the robot and assuming that a speed of 1 mm/s will be sufficient, the Reynolds number for the micro-robot is then:

$$\mathrm{Re} = \frac{2\rho UR}{\mu} \approx 1 \qquad (1)$$

Microorganisms have much smaller Reynolds numbers, but *Re* is still sufficiently small that a similar treatment of the fluid mechanics can be employed.

B. The Resistance-Force Theory

In order to predict the swimming speed and efficiency derived by and the power required for a helical flagellum, resistance-force theory (RFT) can be used to obtain approximate results relatively easily. For an arbitrary filament motion given in Figure 3 defined by $s(l,t)$, whose rotation is symmetric about the direction of travel (x-axis), it is necessary to determine mean swimming speed, induced rotation of the cell or robot, and efficiency. A general formulation of RFT follows.

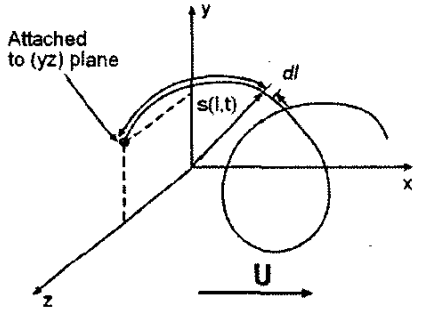

Figure 3: Specification of general filament motion.

The geometry of the filament and robot body as well as the properties of the fluid are taken as given. Here we assume that the filament motion is periodic in time and the filament is attached to the robot body at the y-z plane at all times (Figure 3). Thus, the coordinate system is moving with average velocity U in the $-x$ direction with respect to the rest frame (fluid far from the robot). We also assume that the filament length is constant at all times, corresponding to an inextensible flagellum.

Since this system has a low Reynolds number, we can treat this problem as non-accelerating. Therefore, the force balance in the x direction and the moment balance about the x axis become the following:

$$\frac{1}{\Delta T}\int_0^{\Delta T}\int_0^{L} f_x(l,t)\,dl\,dt + C_D U = 0 \qquad (2)$$

$$\frac{1}{\Delta T}\int_0^{\Delta T}\int_0^{L} [\mathbf{r}\times\mathbf{f}(l,t)]\cdot\mathbf{e}_x\,dl\,dt + C_{D\Omega}\Omega = 0 \qquad (3)$$

Integration is taken over the entire length of the filament (L) and over the smallest time in which the filament motion repeats (ΔT). Integration of the first term in the force balance and the first term in the moment balance yields the thrust force derived and the motor torque required respectively.

So, in order to solve this problem, f must be described. For this reason, a new coordinate system is introduced (Figure 4). At a given point along the filament at an instant of time, the instantaneous filament speed can be decomposed into motion in the direction and that perpendicular to the filament. The important parameters are found by calculating the force per unit length in the normal and tangent directions as a function of l and t.

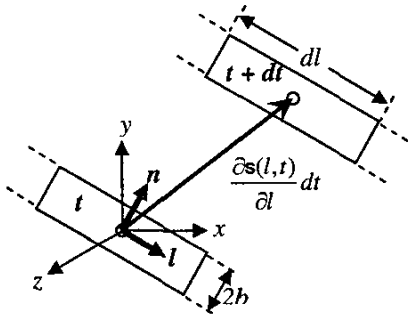

Figure 4: Local coordinate system

C. The Helical Filament Case

A simple case of practical significance to the proposed robot is a rigidly rotating helix attached to the robot at its base as shown in Figure 5.

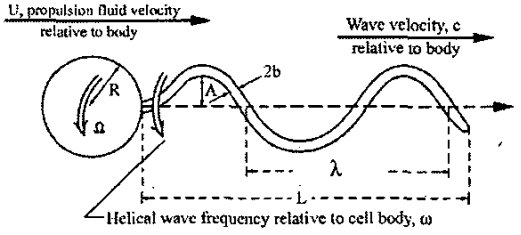

Figure 5: Organism propelled by helical waves

For a rotating helix translating only along its axis of rotation, the kinematics of the motion are identical at all points along the filament. The force and moment balances reduce to the relatively simple expressions:

$$N f_x L + C_D U = 0 \qquad (4)$$

$$N f_y AL + C_{D\Omega}\Omega = 0 \qquad (5)$$

$$C_D = 6\pi\mu R \qquad (6)$$

$$C_{D\Omega} = 8\pi\mu R^3 \qquad (7)$$

The forces in the x and y directions are composed of forces in the normal and tangent directions as:

$$f_x = f_l \cos\theta - f_n \sin\theta \quad (8)$$

$$f_y = f_l \sin\theta + f_n \cos\theta \quad (9)$$

$$\tan\theta = \frac{\lambda}{2\pi A} \quad (10)$$

$$f_l = -C_l (U\cos\theta - \omega A \sin\theta)$$
$$f_n = -C_n (-U\sin\theta - \omega A \cos\theta) \quad (11)$$

Here, C_l and C_n are the resistance coefficients developed by Gray and Hancock [7]:

$$C_l = \frac{2\pi\mu}{\ln\left(\frac{2\lambda}{b}\right) - \frac{1}{2}} \qquad C_n = \frac{4\pi\mu}{\ln\left(\frac{2\lambda}{b}\right) + \frac{1}{2}} \quad (12)$$

These relations define two independent equations of U and Ω. Thrust force, swimming speed and rotation rate are then determined from solving the simultaneous equations. Efficiency η is computed from a ratio of the useful work to the total work input by the motor.

$$\eta = \frac{FU}{T\omega} \quad (13)$$

V. DESIGN OF PROPULSION ACTUATION

The propulsion system will use thin filaments attached perpendicularly to a surface (Figure 6). The filament material should have relatively non-reactive surfaces with strong covalent bonds to minimize any degradation caused by the biological surroundings. In addition, the filament must be sufficiently elastic to allow easy conformation into a helical shape when revolved in a viscous medium yet strong enough to resist wear and torsion fatigue. For these reasons, carbon nanotubes are an ideal choice.

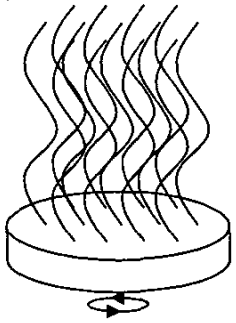

Figure 6: Circular translation of the substrate causes helical waves to propagate.

To act as flagella, carbon nanotubes should be grown vertically on the substrate that will be actuated. Their length should be on the order of magnitude of a hundred microns so that L/b, the aspect ratio, is large.

Xie et al [8, 9] demonstrated a method that allows the fabrication of such carbon nanotubes. Through the use of pyrolysis of acetylene over iron/silica substrates, they were able to produce very long, multiwalled carbon nanotubes that reach about 2 mm in length. According to their method, the final length of the carbon nanotubes depends on the total time of growth: 48 hours are necessary to grow a 2 mm array. Scanning electron microscopy showed that these CNTs grow separately and perpendicularly from the substrate. They present a uniform external diameter (~20-40 nm) with spacing about 100 nm between the tubes. This density is too high, so it would be necessary to pattern a small fraction of the substrate for CNT growth to avoid interaction between filaments.

Given that the CNTs can be grown, estimates of the mechanical properties of such carbon nanotubes are necessary. Falvo et al [10] showed that multiwalled carbon nanotubes can be bent elastically through large angles without undergoing catastrophic failure. They found resistance to high strain deformation and remarkable flexibility and resilience. With an atomic force microscope, they were able to observe bending of CNTs with a radius of curvature as small as 20 nm and strain along the inside and the outside of the tube bend as large as 16%. For the computations, the following properties for multiwalled carbon nanotubes were used: Poisson ratio equal to 0.3 and a Young's modulus between 10 GPa and 100 Gpa [10, 11].

Maneuvering will be accomplished by the use of a four quadrant propulsion system shown from the rear of the robot in Figure 7.

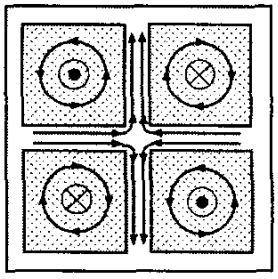

Figure 7: Independent rotation of four plates enables maneuverability.

Here, each plate is resonated at the same amplitude in a circular pattern for normal straight swimming. They revolve in a pattern as shown by the circular arrows on each plate, and the resulting fluid flow is shown with some possible streamlines. The rotating filaments give rise to moments about the direction of travel that are balanced by the torque developed from the viscous drag associated with rotation of the robot. Thus, for straight swimming, two of the plates should rotate one way and the remaining two rotate the other way. Similarly, to rotate the robot, all the plates should rotate in the same direction. To turn, two neighboring plates must be turned off while the other two rotate in opposite directions. For example, to turn right the two right-side plates should be off.

This system contains components of many different scales, significantly increasing the difficulty of fabrication. The robot is on the scale of a millimeter, the filaments and the circularly translating substrates are on the scale of a hundred microns, and the filament radius is about 30 nanometers.

Design parameters with purple

yellow efficiency and performance

VI. Simulations

A. Assumptions

In the following analysis, performed in Matlab (from MathWorks), several additional assumptions were made. End effects at the base and at the tip of the filaments were ignored. Twisting of the filament is also ignored for ease of computation. R is taken as 500 microns, L is 100 microns, b is 30 nm, and viscosity is $7\text{x}10^{-4}$ kg/m.s. The Young's modulus of the filament is taken conservatively as 1 GPa and the poisson ratio is 0.3.

B. Solid Mechanics Program

In order to model the shape that the filament will take under certain conditions, the constitutive relations describing stress and strain in the filament must be incorporated [12, 13].

$$f_n = \kappa n_3 + \tau^2 \kappa \left(\frac{E_y}{2 - 2\nu - 4\nu^2} \right) \tag{17}$$

$$\kappa = \frac{A}{(\lambda/2\pi)^2 + A^2} \tag{18}$$

$$\tau = \frac{\lambda/2\pi}{(\lambda/2\pi)^2 + A^2}$$

The filament is modeled as an isotropic linear elastic material and only bending is considered. By balancing stresses within the filament with the viscous forces derived from filament motion, the geometry that the filament will take was computed.

C. Graphs

Figure 1 shows that a maximum in efficiency is present for θ approximately equal to 45 degrees. This finding has been previously confirmed [14]. The efficiency in this case is completely independent of ω since both A and θ have been specified (i.e. filament bending is not computed).

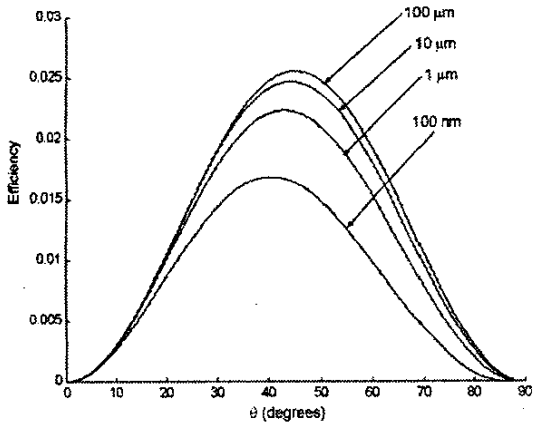

Figure 8: Efficiency as a function of θ for different values of A

In Figure 9, it is apparent that an optimum value of N exists for a given A. This is due to the existence of a maximum swimming speed. As the robot gains speed, the fluid velocity at the filament surface decreases with respect to the moving robot. Therefore, each additional increase in speed requires a greater increase in frequency. This causes the motor torque to rise faster than the swimming speed, thereby decreasing overall efficiency.

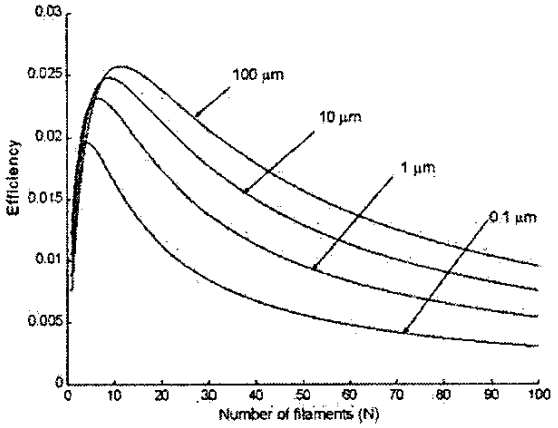

Figure 9: Efficiency as a function of N for different values of A (θ = 45°)

In Figure 10, efficiency is plotted as a function of A at constant ω. This plot shows that as ω is increased, the ideal helical wave amplitude decreases. The increased viscous forces which bend the filament greatly at high frequency dictate that for efficient behavior, A must not exceed values that will bend the filament into much more than a 45 degree helix angle.

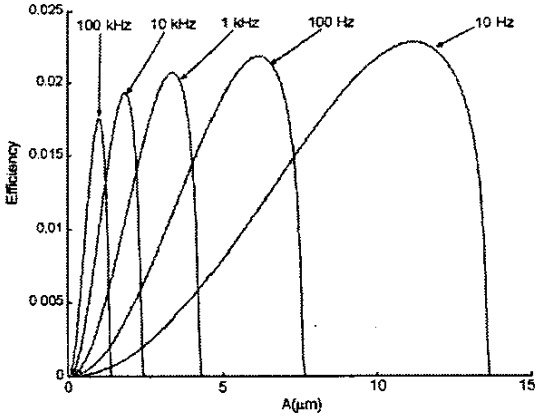

Figure 10: Efficiency as a function of A for different values of ω

In Figure 10, U is plotted on a log scale as a function of A at constant ω. This plot shows that satisfactory swimming speeds can be attained over the ranges that are also most efficient (it should be noted that the data that corresponds to speeds above 1mm/s starts to violate the assumption of stokes flow). In addition, as ω is increased, the maximum U increases. This is a result of the increased relative stiffness of the filament that is tightly coiled as opposed to that of the

filament that has a much higher A. The stiffer behavior allows higher viscous forces and hence thrust.

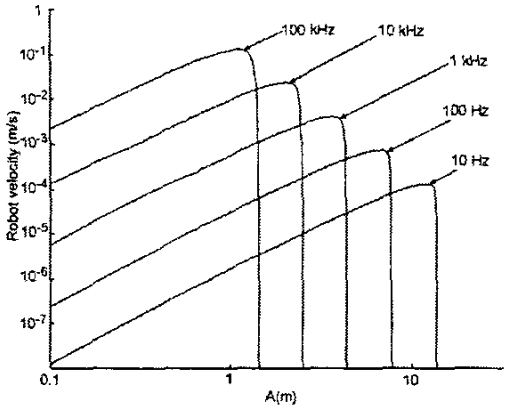

Figure 11: Log-Log graph of U as a function of A for different ω (N=10)

A cursory analysis suggests that a comb drive could be used to obtain a high efficiency of propulsion. For a reasonable displacement ($2A$) of 10 microns at 100 Hz, a swimming speed of half a millimeter per second is predicted. In addition, for these parameters, 2% efficiency is calculated. Assuming that the comb drive is able to operate at a torque of 130 μN·nm and with an efficiency of 0.1%, the total power required would be about 1 nW.

VII. CONCLUSION

This paper proposes a novel *in-vivo* biomimetic swimming micro-robot for destroying kidney stones in a minimally invasive way. Design aspects are discussed, and an analysis of propulsion is presented. This robot will be at the millimeter scale and function in the fluid of the human renal system, so that for realistic swimming speeds the flow surrounding the robot is at low Reynolds number. Nature has engineered a solution for this type of flow: the use of cilia and flagella in bacteria and spermatozoa. This inspired the design of the propulsion system for the micro-robot.

Locomotion via an array of multi-walled carbon nanotubes grown vertically from a surface is achieved by circular translation of the substrate. Possibly enabled by a set of comb drives, this causes the propagation of a helical wave along the filaments.

The E. coli bacterium is able to swim at about 30μm/s with a thrust force of half a piconewton at a fraction of 1% efficiency. The analysis of propulsion with respect to the viscous forces from the fluid and the bending of the synthetic filaments gives promising results. While some simplifications were made in the model, the proposed robot compares well with the bacterium. The robot would be capable of traveling at almost 1mm/s with a 2% hydrodynamic efficiency for 1nW of power, with 100μm-long filaments. This suggests that it is possible to provide the energy to propel such a micro-robot. However, the energy required to destroy a kidney stone would be much larger and the design of the destruction mechanism will be another challenge. If piezoelectric actuators are used to destroy the kidney stone, a wave-guide to amplify the shockwave would be necessary [15]. This would also require a capacitor to store the energy to generate this spark and a way to protect the micro-robot against the energy of the spark.

The analysis presented leads to the conclusion that although implementation may be difficult, the use of carbon nanotubes as synthetic flagella for a swimming micro robot can be a very effective means of locomotion. Although this design is by its nature long-term, kidney stones represent on of the most important health problems in the world. Fortunately, from an engineering perspective the renal system is one of the simplest environments in which a micro robot can function within the body. Consequently, successful microrobotic destruction of kidney stones may open the door to further clinical applications.

VIII. REFERENCES

[1] S. Guo, Y. Hasegaw, T. Fukuda, and K. Asaka, "Fish-like underwater microrobot with multi DOF," presented at International Symposium on Micromechatronics and Human Science, Piscataway, NJ, USA, 2001.

[2] S. Guo, T. Fukuda, and K. Asaka, "A new type of fish-like underwater microrobot," *Ieee/Asme Transactions on Mechatronics*, vol. 8, pp. 136-141, 2003.

[3] G. Laurent and E. Piat, "Efficiency of Swimming Microrobots using Polymer Metal Composite Actuators," presented at IEEE Robotics and Automation Conference, Seoul, Korea, 2001.

[4] D. Howard and B. Sturtevant, "In vitro Study of the Mechanical Effects of Shock-Wave Lithotripsy," *Ultrasound in Medecine and Biology*, vol. 23, pp. 1107-1122, 1997.

[5] H. Nishikawa, T. Sasaya, T. Shibata, T. Kaneko, N. Mitumoto, S. Kawakita, and N. Kawahara, "In-Pipe Wireless Micro Locomotive System," presented at International Symposium on Mechatronics and Human Science, Nagoya, Japan, 1999.

[6] E. M. Purcell, "Life at low Reynolds Number." Cambridge, 1977.

[7] C. Brennen and H. Winet, "Fluid Mechanics of Propulsion by Cilia and Flagella," *Annual review of Fluid Mechanics*, vol. 9, pp. 339-398, 1977.

[8] S. S. Xie, W. Z. Li, Z. W. Pan, B. H. Chang, and L. F. Sun, "Carbon nanotube arrays," *The European Physical Journal D*, vol. 9, pp. 85-89, 1999.

[9] Z. W. Pan, S. S. Xie, B. H. Chang, C. Y. Wang, L. Lu, W. Liu, W. Y. Zhou, W. Z. Li, and L. X. Qian, "Very long carbon nanotubes," *Nature*, vol. 394, pp. 631-632, 1998.

[10] M. R. Falvo, G. J. Clary, R. M. Taylor II, V. Chi, F. P. Brooks Jr, S. Washburn, and R. Superfine, "Bending and buckling of carbon nanotubes under large strain," *Nature*, vol. 389, pp. 582-584, 1997.

[11] R. H. Baughman, A. A. Zakhidov, and W. A. de Heer, "Carbon Nanotubes-The Route toward Applications," *Science*, vol. 297, pp. 787-792, 2002.

[12] B. Armbruster and A. Goriely, "Static solutions of an elastic rod in a helical shape without twist," University of Arizona 2002.

[13] M. Nizette and A. Goriely, "Towards a classification of Euler Kirchhoff filaments," University of Arizona.

[14] J. J. L. Higdon, "The Hydrodynamics of flagellar propulsion: Helical waves," *Journal of Fluid Mechanics*, vol. 94, pp. 331-351, 1979.

[15] G. Montaldo, "Generation of very high pressure pulses with 1-bite time reversal in a solid waveguide," *J. Acoust. Soc. Am*, vol. 110, pp. 2849-2857, 2001.